Macromolecules

pubs.acs.org/Macromolecules Article

Rate-Dependent Damage Mechanics of Polymer Networks with Reversible Bonds

Samuel C. Lamont, Jason Mulderrig, Nikolaos Bouklas, and Franck J. Vernerey*

Cite This: *Macromolecules* 2021, 54, 10801−10813 Read Online

ACCESS | Metrics & More | Article Recommendations | Supporting Information

ABSTRACT: Dynamic polymer networks utilize weak bonding interactions to dissipate the stored energy and provide a source of self-healing for the material. Due to this, tracking the progression of damage in these networks is poorly understood as it becomes necessary to distinguish between reversible and irreversible bond detachment (by kinetic bond exchange or chain rupture, respectively). In this work, we present a statistical formulation based on the transient network theory to track the chain conformation space of a dynamic polymer network whose chains rupture after being pulled past a critical stretch. We explain the predictions of this model by the observable material timescales of relaxation and self-healing, which are related to the kinetic rates of attachment and detachment. We demonstrate our model to match experimental data of cyclic loading and self-healing experiments, providing physical interpretation for these complex behaviors in dynamic polymer networks.

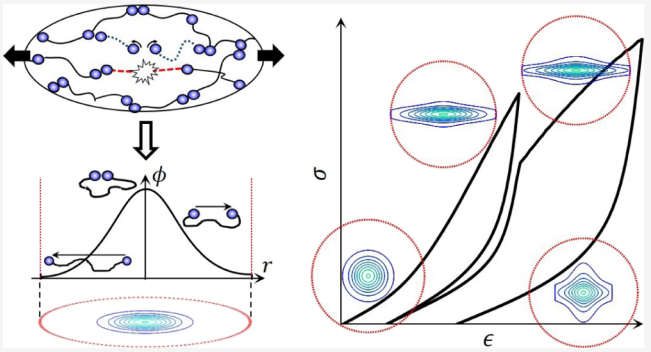

1. INTRODUCTION

Soft materials, such as hydrogels, polymers, and biological tissues, display a rich spectrum of mechanical responses, in terms of elasticity, fracture resistance, and stimuli responsiveness. This is today at the heart of a number of emerging applications spanning soft robotics,[1] tissue engineering,[2−4] and stretchable electronics.[5] In almost all of these applications, it is highly desirable to design materials that are not only resistant to damage and fracture but that can also self-heal over time. Tremendous efforts have been invested to enhance damage resistance through a variety of strategies, including particle reinforcement,[6,7] sacrificial bond breaking,[4,8,9] or the introduction of reversible bonds.[10−12] Despite the differences in methodologies, a common objective has been to introduce some energy dissipation mechanism that can delay or even prevent the initiation and catastrophic proliferation of network damage.[13] Among these strategies, the introduction of a transient network has been favored by many researchers due to the capability of bond reformation, leading to mechanical strength recovery after large deformation[14] and self-healing after cutting.[12] The introduction of these dynamic networks yields a multitude of new questions regarding the physical origins of damage. Indeed, if damage has traditionally been described as the rupture (or detachment) of a chain from the network, then what distinguishes bond dissociation from chain damage? Furthermore, damage is often defined as the irrecoverable loss of network connectivity over time. This condition clearly does not apply to transient networks since bond reattachment is possible, as observed during self-healing.

To better apprehend the distinction between bond dynamics and chain rupture, let us first consider damage in a covalent network. In this case, the primary failure mechanism is the rupture of individual chains or cross-links when they are stretched beyond their load-carrying capacity.[15,16] This usually occurs when their end-to-end distance is close to their contour length, where chains undergo a pronounced stiffening. At the network level, this is manifested by progressive failure, which eventually leads to localized macroscopic failure events such as cracking. In contrast, the stretch of a chain in a transient network does not necessarily follow the deformation of the bulk; for instance, if loading is applied slowly enough, a chain may first stretch with the network before it dissociates from it due to ambient thermal fluctuations (Figure 1). In this case, the dissociated chains may reassociate in a more favorable (force-free) state that will protect them from reaching their critical stretch. In essence, bond dynamics should therefore delay or even completely prohibit damage initiation under certain rates of deformation.

Models for the progression of damage in elastic polymers, such as rubbers and other elastomers, have been primarily used

Received: September 13, 2021
Revised: November 18, 2021
Published: December 1, 2021

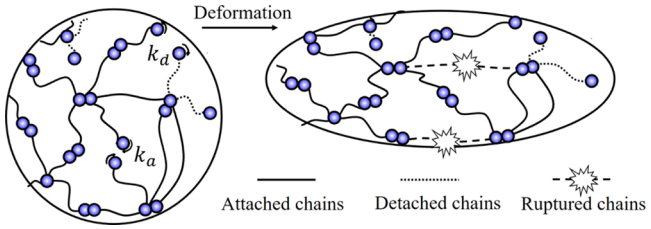

Figure 1. Distinction between chain rupture and chain detachment in a transient network. In this network, a chain can be found in three distinct states: attached, detached, and ruptured. The ruptured chains are unable to create new network connections and are at the origin of irreversible damage.

to study fracture or rate-independent softening.[1] In order to properly account for the fact that chain rupture is driven by the stretching of bonds, as emphasized by the foundational work of Lake and Thomas,[21] Mao et al. incorporated stretchable bonds and the internal energy of bond stretching into a micro-mechanical framework for chain rupture.[15] This framework has been extended to investigate the mechanics of progressive chain rupture,[19,20,22] the Mullins effect,[18] and damage in polydisperse networks[16,23−25] to name a few. On the other hand, micro-mechanical models for viscoelasticity typically consider time dependence as stemming from the existence of weak bonds that constantly break and reform throughout the network. Such formulations were originally proposed for reptation in polymer melts[26,27] but have been extended to study rubbery viscoelasticity[28,29] and the mechanics of dynamic polymer networks.[30,31] Notably, recent work by Buche and Silberstein[32] accounted for force-sensitive reversible bond breaking through an intact chain probability density distribution that evolves through time. Some studies have been performed to combine the ideas of these previous works,[33,34] but the formulations are typically complex, empirical, or both, which inhibits a greater understanding of the underlying mechanisms. Thus, while the individual topics of viscoelasticity and damage in polymer networks have been studied extensively, as of yet there has been little work on investigating their coupled behavior.

In this work, we develop a statistical theory of damage for transient networks that can directly bridge the molecular mechanisms and macroscopic response. As described in earlier studies,[17,31] the theory starts from the description of the physical state of a polymer network using a statistical distribution of the length and direction of the end-to-end vectors of its physically connected chains. The transient network theory (TNT) provides an evolution law for this distribution (in the form of a Fokker−Planck equation) as a response to the application of a macroscopic deformation and molecular-level events causing chain detachment and reattachment.[31] In addition to these mechanisms, we here incorporate the phenomenon of chain damage as a chain reaches its critical stretch, which, as will be seen, modifies the original Fokker−Planck equation by adding a rate of chain rupture over time. The knowledge of this distribution over time then allows us to directly evaluate the stored elastic energy, dissipation rates (that is manifested as viscoelasticity and damage), and the stress tensor. The final model is able to capture the evolution of rate-dependent and anisotropic damage in transient networks. With this aim, Section 2 presents the statistical framework and general thermodynamic arguments for the model. Section 3 introduces a rupture criterion for flexible chains, leading to a specific form of the damage model. We then provide details on the numerical solution procedure for the model and illustrate model predictions for basic conditions and loading scenarios. Finally, in Section 4, we provide a comprehensive overview of the model and compare its predictions with published experimental data.

2. STATISTICAL MECHANICS OF DAMAGE IN TRANSIENT NETWORKS

Here, we seek to describe the evolution of a dynamic network made of long flexible chains composed of N freely rotating joined Kuhn segments with an initial reference length b. These chains are connected at cross-linking points by reversible bonds that possess their own association and dissociation rates. The nature of such a network entails that its chains can be characterized by three distinct states (Figure 1): (a) an "effective state" where the chain is connected to the network and effectively bears load, (b) a "detached state" where the chain is still intact but is disconnected from the network and thus is unable to carry load, and finally (c) a "ruptured state", where the chain can never regain its effectiveness in carrying load. Because the last two categories are mechanically ineffective, we may only describe their presence through nominal concentrations C_d (for detached) and C_r (for ruptured), respectively. If the concentration of effective chains is C, the concentration of all chains in the network is C_{tot}, and assuming that the total number of chain is conserved, we have

$$C + C_d + C_r = C_{tot} \tag{1}$$

$$\dot{C} + \dot{C}_d + \dot{C}_r = 0 \tag{2}$$

where a superimposed dot is used to designate a material time derivative. Because they are mechanically active, the effective chains must be described not only by their concentration but also by the spatial conformation of their end-to-end vector $\boldsymbol{r}$. We capture this by following the probability function $p(\boldsymbol{\lambda})$ of their normalized end-to-end vector $\boldsymbol{\lambda} = \boldsymbol{r}/r_0$, where $r_0 = \sqrt{N}b$ is the root-mean-square average end-to-end distance of the

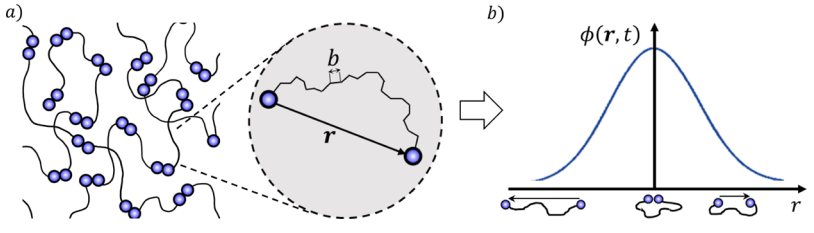

Figure 2. (a) End-to-end vector of a polymer chain, defined as the vector spanning two cross-links. (b) Distribution density $\phi(\boldsymbol{r}, t)$ of a (one-dimensional) network conformation.

https://doi.org/10.1021/acs.macromol.1c01943
Macromolecules 2021, 54, 10801−10813

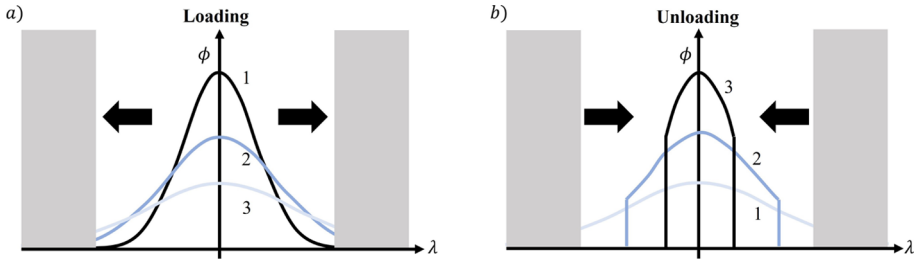

Figure 3. Evolution of the (one-dimensional) chain distribution during (a) loading and (b) unloading. Numbers 1, 2, and 3 indicate different time steps in the loading history. The gray regions on the conformation space represent the stretches that induce chain rupture.

chains in the undeformed network (Figure 2). The quantities C and p can be combined into the distribution

$$\phi(\boldsymbol{\lambda}, t) = C(t)p(\boldsymbol{\lambda}, t) \tag{3}$$

This function indicates the density of effective chains in a given conformation $\boldsymbol{\lambda}$. The nominal concentration of effective chains can then be back-calculated from the knowledge of the distribution

$$C(t) = \int_{\Omega} \phi(\boldsymbol{\lambda}, t)\mathrm{d}\Omega \tag{4}$$

where $\int_{\Omega}\phi \mathrm{d}\Omega$ is the integral of the chain distribution ϕ over the space of all possible conformations, Ω: $\{\boldsymbol{\lambda} \in \mathbb{R}^3\}$.

2.1. Fokker–Planck Equation for Network Evolution. The chain distribution ϕ is considered to evolve according to external stimuli as well as internal topological rearrangement. For simplicity, we assume an instantaneously affine kinematic law such that a chain in the network transforms according to $\dot{\boldsymbol{\lambda}} = \mathbf{L}\boldsymbol{\lambda}$, where $\boldsymbol{L} = \dot{\boldsymbol{F}}\boldsymbol{F}^{-1}$ is the macroscopic velocity gradient and $\boldsymbol{F}$ is the deformation gradient. We also assume that effective chains dissociate from the network following a first-order kinetics law with constant k_d, while dissociated (but intact) chains may reattach in a relaxed state following a similar law with kinetic constant k_a. From these two assumptions, Vernerey et al.[31] derived an evolution equation for ϕ of the form

$$\frac{\partial \phi}{\partial t} = -\mathbf{L}\colon\left(\frac{\partial \phi}{\partial \boldsymbol{\lambda}} \otimes \boldsymbol{\lambda}\right) - \phi \mathrm{Tr}(\mathbf{L}) + k_a C_d p_0 - k_d \phi \tag{5}$$

where $\otimes$ is the dyadic (tensor) product and p_0 is the stress-free probability density function of a single chain. The introduction of a criterion for chain rupture is quite natural with this formalism. Indeed, the assumption that a chain breaks when its deformation reaches a critical stretch value λ_c translates into the following condition for the distribution ϕ

$$\phi(\boldsymbol{\lambda}, t) = 0 \qquad \text{when } |\boldsymbol{\lambda}| > \lambda_c \tag{6}$$

This statement enforces that the density of chains whose stretch is larger than λ_c must vanish. If the initial distribution $\phi(\boldsymbol{\lambda}, 0)$ is known, eq 5 can then be integrated in time under the restriction imposed by eq 6 in order to determine the distribution ϕ at any time during its loading history. To close the model, we now need to determine the evolution of the detached chain concentration C_d that enters the third term on the right-hand side of eq 5. From eq 2, it is found as

$$\dot{C}_d = -(\dot{C} + \dot{C}_r) \tag{7}$$

The evolution of attached chains follows from eq 4. Imposing the restriction of eq 6 defines a new domain Ω_u: $\{\boldsymbol{\lambda} \in \Omega, |\boldsymbol{\lambda}| < \lambda_c\}$, which is the conformation space of undamaged chains in the network. Integrating the Fokker–Planck equation over Ω_u and using the divergence theorem, we find

$$\dot{C} = -\mathbf{L}\colon\int_{\Omega_u}\left(\frac{\partial \phi}{\partial \boldsymbol{\lambda}} \otimes \boldsymbol{\lambda}\right)\mathrm{d}\Omega - C\mathrm{Tr}(\mathbf{L}) + k_a C_d - k_d C$$

$$\dot{C} = -\int_{\Gamma_u}(\mathbf{j}\cdot\mathbf{n})\mathrm{d}S + k_a C_d - k_d C \tag{8}$$

where Γ_u is the boundary of the damage surface, $|\boldsymbol{\lambda}| = \lambda_c$, and $\mathbf{j} = \phi\dot{\boldsymbol{\lambda}}$ is introduced. The vector $\boldsymbol{j}$ is interpreted as the flux of chains through the conformation space during deformation. This flux represents the evolution of chains toward a preferred conformation when a loading is applied (see Figure 3). The first term of eq 8 expresses the fact that the rate of chain loss (from rupture) in the network is equal to the flux of effective chains crossing the damage surface. We may therefore define the rate of chain rupture as

$$\dot{C}_r = \int_{\Gamma_u}(\mathbf{j}\cdot\mathbf{n})\mathrm{d}S \tag{9}$$

while the last two terms in eq 8 denote a change in effective concentration due to bond dynamics. Combining eqs 7–9, the rate of the detached chain concentration is simply

$$\dot{C}_d = -k_a C_d + k_d C \tag{10}$$

2.2. Second Principle, Energy Dissipation, and Stress. We would next like to explore the constitutive predictions of the model, starting at the level of a single chain. When the network is deformed, chains store energy due to conformational changes and enthalpic interactions. Keeping things general for now, let us introduce ψ_c as the Helmholtz free energy in a flexible chain. Summing over the space of undamaged chain conformations, the elastic energy ψ stored per unit network volume is found as

$$\psi = \int_{\Omega_u}\phi\psi_c\,\mathrm{d}\Omega = C\int_{\Omega_u}p\psi_c\,\mathrm{d}\Omega = C\langle\psi_c\rangle \tag{11}$$

where the notation $\langle\cdot\rangle$ defines the statistical average over the conformation space of effective chains. The free-energy density ψ can thus be used to relate the current chain conformation (represented by the distribution $\phi(\boldsymbol{r}, t)$) to macroscopic quantities such as stress and energy dissipation. For this, we first introduce the Clausius–Duhem inequality to enforce the second law of thermodynamics. Considering an isothermal process and assuming incompressible deformation, it is written as

$$\mathcal{D} = (\boldsymbol{\sigma} - \pi\mathbf{I})\colon\mathbf{L} - \dot{\psi} \geq 0 \tag{12}$$

https://doi.org/10.1021/acs.macromol.1c01943
Macromolecules 2021, 54, 10801–10813

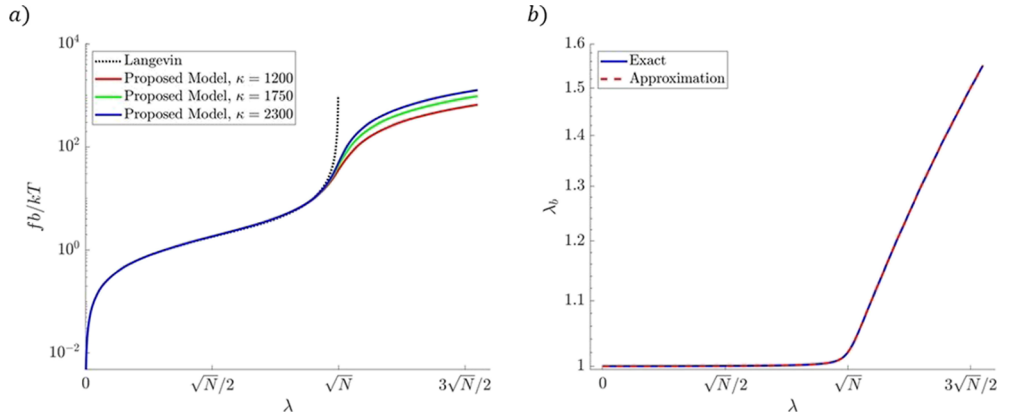

Figure 4. (a) Comparison of the inextensible Langevin chain force (dashed lines) with extensible Langevin chain forces (solid lines) with differing values of bond stiffness E_b normalized by kT, $\kappa = E_b/(kT)$. All chain force values are normalized by kT/b. Beyond the extensibility limit, the chain force increases as bond stiffness increases. (b) Comparison of the approximated solution of the Kuhn segment stretch using the Bergstrom approximation with the solution of the Kuhn segment stretch using the exact inverse Langevin function (κ = 2300 is used here).

where $\mathcal{D}$ is the rate of energy dissipation per unit volume and π is the Lagrange multiplier enforcing the incompressibility constraint. Its physical meaning can be interpreted as a hydrostatic stress-like quantity that prevents volume change. Using eq 5, the rate of change of elastic energy density, $\dot{\psi}$, is found as

$$\begin{aligned}\dot{\psi} &= \int_{\Omega_u} \dot{\phi}\psi_c \, d\Omega \\ &= -\int_{\Omega_u} \left(\frac{\partial \phi}{\partial \boldsymbol{\lambda}}\cdot\dot{\boldsymbol{\lambda}}\right)\psi_c \, d\Omega - \psi \mathrm{Tr}(\mathbf{L}) + k_a C_d \langle\psi_c\rangle_0 \\ &\quad - k_d C\langle\psi_c\rangle\end{aligned}$$

where $\langle\psi_c\rangle 0 = \int_{\Omega_u} p_0 \psi_c d\Omega$ is the average energy in a stress-free chain, taken about the reference probability density function p_0. Changes in stored energy are thus due to three mechanisms: (i) elastic distortion of the chains, (ii) detachment events, which release stored energy, and (iii) attachment events, which reset the deformation. As the distribution $\phi(\boldsymbol{r}, t)$ is defined for all chain conformations Ω, we should further break down the first term to explicitly account for chains leaving the region Ω_u as they immediately damage as per eq 6. Using integration by parts and the divergence theorem, we define

$$\begin{aligned}&\int_{\Omega_u} \left(\frac{\partial \phi}{\partial \boldsymbol{\lambda}}\cdot\dot{\boldsymbol{\lambda}}\right)\psi_c \, d\Omega \\ &= \int_{\Gamma_u} \mathbf{q}\cdot\mathbf{n} \, dS - \int_{\Omega_u} \phi \mathbf{f}_c \cdot \dot{\boldsymbol{\lambda}} \, d\Omega - \psi \mathrm{Tr}(\mathbf{L})\end{aligned} \tag{13}$$

where we introduce $\boldsymbol{q} = \phi\psi_c\dot{\boldsymbol{\lambda}} = \psi_c \boldsymbol{j}$ as the chain energy flux through the conformation space and $\boldsymbol{f}_c = d\psi_c/d\boldsymbol{\lambda}$ as the force vector of a single chain. The rate of change in free energy then becomes

$$\begin{aligned}\dot{\psi} &= -\int_{\Gamma_u} \mathbf{q}\cdot\mathbf{n} \, dS + \left(\int_{\Omega_u} \phi \mathbf{f}_c \otimes \boldsymbol{\lambda} \, d\Omega\right) : \mathbf{L} + k_a C_d \langle\psi\rangle_0 \\ &\quad - k_d C\langle\psi\rangle\end{aligned} \tag{14}$$

Note the disappearance of terms involving TrL as chains leaving the volume (due to chain rupture) are captured by the integral over the boundary Γ_u. Combining eqs 12 and (14), we identify the true (Cauchy) stress as

$$\sigma = \int_{\Omega_u} \phi \mathbf{f}_c \otimes \boldsymbol{\lambda} \, d\Omega + \pi \mathbf{I} \tag{15}$$

The remaining terms represent the energy dissipation of the network. In this case, two independent processes dissipate energy: chain dynamics and bond rupture. The dissipation $\mathcal{D}$ can thus be additively decomposed into $\mathcal{D} = \mathcal{D}_d + \mathcal{D}_r$, where the terms $\mathcal{D}_d$ and $\mathcal{D}_r$ correspond to dissipation associated with chain dynamics and chain rupture, respectively. These are identified from eq 14 as

$$\mathcal{D}_r = \int_{\Gamma_u} \mathbf{q}\cdot\mathbf{n} \, dS \tag{16}$$

$$\mathcal{D}_d = k_d C\langle\psi\rangle - k_a C_d \langle\psi\rangle_0 \tag{17}$$

Considering these as isolated processes, the Clausius–Duhem inequality should enforce that both $\mathcal{D}_r$ and $\mathcal{D}_d$ be nonnegative. The constraint on $\mathcal{D}_r$ is trivially satisfied as chains cannot rupture during unloading. This places the following restriction on the system:

$$k_d C\langle\psi\rangle \geq k_a C_d \langle\psi\rangle_0 \tag{18}$$

Physically, this reflects the fact that the system cannot gain energy from attachment events. This is true for most physical systems and has been discussed in previous works.[35] We particularly note that this inequality remains satisfied when considering the sensitivity of bond detachment to external forces,[36] which is explicitly discussed in the context of the TNT by Lamont and Vernerey.[37]

3. DAMAGE MECHANICS OF A NONLINEAR MOLECULAR NETWORK

So far, we have presented the model in general terms to promote a wider understanding of the governing physics. In this section, we introduce the specifics of our implementation and basic predictions the model provides. Starting at the level of a single chain, we incorporate an enthalpic term to account for the stretching of Kuhn segments and eventual bond rupture. We then define a thermodynamically consistent reference distribution p_0 and end with the basic predictions of the model.

3.1. Single-Chain Response and Rupture. Chain rupture usually occurs when a chain is stretched toward its

https://doi.org/10.1021/acs.macromol.1c01943
Macromolecules 2021, 54, 10801−10813

contour length (i.e., $\lambda \to \sqrt{N}$), at which point the Kuhn segments are forced to align in the direction of stretch. Adopting the inextensible Langevin chain model, which assumes rigid Kuhn segments, the force-extension response of the chain exhibits severe stiffening behavior (see the left panel in Figure 4) since the Kuhn segments cannot accommodate any further displacement once they are aligned in the direction of stretch. However, adopting the extensible Langevin chain model assumes that each Kuhn segment along the chain can stretch to a length b^{ext} when the chain as a whole is stretched toward and beyond its contour length, which may eventually cause its rupture.[15,38] By defining the Kuhn segment stretch as $\lambda_b = b^{ext}/b$, we define the form of the Helmholtz free energy of the chain to be

$$\psi_c(\lambda, \lambda_b) = \mathcal{U}(\lambda_b) - T\mathcal{S}(\lambda, \lambda_b) \tag{19}$$

This approximation assumes that the energetic contributions of enthalpy and entropy along the chain are decoupled, which was first proposed by Mao et al.[15] According to Figure 4a, the extensible Langevin chain model in eq 19 deviates from the inextensible Langevin chain model at high chain stretches ($\lambda \geq 0.9\sqrt{N}$). The entropic contribution of the chain, $\mathcal{S}(\lambda, \lambda_b)$, is typically captured by the inverse Langevin function, $\mathcal{L}^{-1}$. Due to the implicit nature of this function, it is however more convenient to work with its Padé approximation, as introduced by Cohen,[39] $\mathcal{L}^{-1}(x) \approx x(3 - x^2)/(1 - x^2)$. With this approximation, the entropy of the chain can be written[40,41]

$$\mathcal{S} = -Nk\left[\frac{1}{2}\left(\frac{\lambda}{\sqrt{N}\lambda_b}\right)^2 - \ln\left(1 - \left(\frac{\lambda}{\sqrt{N}\lambda_b}\right)^2\right)\right] \tag{20}$$

where the term λ/λ_b is interpreted as the entropic stretch, that is, the contribution that arises only from the realignment of Kuhn segments in the direction of chain extension. In contrast, the stretching of Kuhn segments is an enthalpic process that finds its source in the molecular distortion of bonds in the chain backbone. This enthalpic contribution can be chosen as a harmonic potential of the form

$$\mathcal{U}(\lambda_b) = \frac{NE_b}{2}(\lambda_b - 1)^2 \tag{21}$$

where E_b is the elastic stiffness of each molecular bond in the chain backbone. All together, the free energy of the chain takes the form

$$\psi_c(\lambda, \lambda_b) = N\left\{\frac{E_b}{2}(\lambda_b - 1)^2 + kT\left[\frac{1}{2}\left(\frac{\lambda}{\sqrt{N}\lambda_b}\right)^2 - \ln\left(1 - \left(\frac{\lambda}{\sqrt{N}\lambda_b}\right)^2\right)\right]\right\} \tag{22}$$

The chain force is then found as the conjugate of the end-to-end distance r or alternatively the applied chain stretch λ as

$$f(\lambda, \lambda_b) = \frac{1}{\sqrt{N}b}\frac{\partial\psi_c(\lambda, \lambda_b)}{\partial\lambda} = \frac{kT}{\lambda_b b}\left(\frac{\lambda}{\sqrt{N}\lambda_b}\right)\frac{\lambda^2 - 3N\lambda_b^2}{\lambda^2 - N\lambda_b^2} \tag{23}$$

where the Kuhn segment stretch λ_b minimizes the free energy ψ_c, that is, $\frac{\partial\psi_c(\lambda, \lambda_b)}{\partial\lambda_b} = 0$. Using the expression for ψ_c, this yields the relation

$$E_b\lambda_b(\lambda_b - 1) = f(\lambda, \lambda_b)\frac{\lambda}{\sqrt{N}}b \tag{24}$$

This is a highly nonlinear equation that requires the derivation of a numerical solution. To enable the derivation of a closed-form solution without sacrificing accuracy, we follow Li and Bouklas[16] and replace the Padé approximation of the inverse Langevin function in the chain force $f(\lambda, \lambda_b)$ with the Bergstrom approximation $\mathcal{L}^{-1} \approx 1/(\text{sign}(x) - x)$ provided that $0.841\,36 \leq |x| < 1$.[29] Since $\lambda > 1$, when $\lambda/\sqrt{N} > 1$, then $\lambda/(\sqrt{N}\lambda_b) < 1$ is always true, validating the use of the Bergstrom approximation. With this approximation, the free-energy minimization problem reduces to the following cubic polynomial:

$$A\lambda_b^3 + \tilde{B}\lambda_b^2 + C\lambda_b + \tilde{D} = 0$$

$$\tilde{A} = \kappa, \qquad \tilde{B} = -\kappa\left(1 + \frac{\lambda}{\sqrt{N}}\right), \qquad \tilde{C} = \kappa\frac{\lambda}{\sqrt{N}},$$

$$\tilde{D} = -\frac{\lambda}{\sqrt{N}}$$

where $\kappa = E_b/(kT)$. With $\tilde{B} - \tilde{A}\tilde{C} > 0$, the Kuhn segment stretch λ_b takes on the value of the following real cubic root:[42]

$$\lambda_b = 2\sqrt{-\frac{r}{3}}\cos\left(\frac{1}{3}\arccos\left(\frac{3s}{2r}\sqrt{-\frac{3}{r}}\right)\right) - \frac{\tilde{B}}{3\tilde{A}} \tag{25}$$

$$r = \frac{3\tilde{A}\tilde{C} - \tilde{B}^2}{3\tilde{A}^2}, \qquad s = \frac{2\tilde{B}^3 - 9\tilde{A}\tilde{B}\tilde{C} + 27\tilde{A}^2\tilde{D}}{27\tilde{A}^3} \tag{26}$$

The right panel of Figure 4 shows how the approximate solution to the Kuhn segment stretch is essentially identical to the exact solution over the entire chain stretch region (even for $\lambda/(\sqrt{N}\lambda_b) < 0.84136$). Note that the solution for the Kuhn segment stretch (and therefore the chain force) is dependent on the bond stiffness. According to the left panel of Figure 4, when a chain is stretched past its extensibility limit, the chain exhibits an increased force for an increase in bond stiffness. To provide a criterion for chain failure, we follow the work of Mao et al.[15] and postulate that a chain ruptures when the elastic energy stored in a Kuhn segment reaches a critical value $(\mathcal{U}_b)_c$. Using eq 21, this can be translated into a criterion for the critical Kuhn segment stretch as

$$(\lambda_b)_c = 1 + \sqrt{\frac{2(\mathcal{U}_b)_c}{NE_b}} \tag{27}$$

This yields the following critical chain stretch:

$$\lambda_c = ker\ \mathcal{A}(\lambda_c) \tag{28}$$

$$\mathcal{A}(\lambda_c) := \left\{\frac{\partial\psi_c}{\partial\lambda_b}(\bar{\lambda}, \bar{\lambda}_b),\ \bar{\lambda} = \bar{\lambda}_c,\ \bar{\lambda}_b = (\bar{\lambda}_b)_c\right\} \tag{29}$$

In this way, an enthalpic-based criterion is used to completely define chain rupture, complying with the observations of Lake and Thomas.[21]

https://doi.org/10.1021/acs.macromol.1c01943
Macromolecules 2021, 54, 10801−10813

3.2. Reference Probability Density Function. We have seen earlier that the chain distribution can only be determined if the reference probability density function is known. This function indeed appears in eq 5 but is also taken as a good guess for the initial distribution $\phi(\boldsymbol{\lambda}, 0)$. While a multivariate Gaussian function is often invoked,[43,44] in this work, we utilize a probability density function that is consistent with the free energy defined in eq 22. This function reads

$$p_0(\boldsymbol{\lambda}) = \frac{1}{\bar{\mathcal{Z}}} \exp\left(-\frac{\psi_c}{kT}\right) \tag{30}$$

where $\bar{\mathcal{Z}}$ is a normalization constant. This connection was discussed by Buche and Silberstein,[45] who studied the efficacy of such approximations over varying chain lengths and stiffness. For simplicity, we omit the enthalpic term in the evaluation of the probability density function, noting that its significance is only relevant at low link stiffness.[45] The resulting change in the final shape of the function p_0 is therefore expected to be minimal. With this in mind, one can show that substituting the expression for ψ_c from eq 22 in eq 30 yields

$$p_0(\boldsymbol{\lambda}) = \frac{\mathcal{H}(|\boldsymbol{\lambda}| + \lambda_c)}{\bar{\mathcal{Z}}} (\boldsymbol{\lambda}\cdot\boldsymbol{\lambda} - N)^N \exp\left(-\frac{\boldsymbol{\lambda}\cdot\boldsymbol{\lambda}}{2}\right) \tag{31}$$

where the Heaviside step function $\mathcal{H}$ was added to restrict the domain of p_0 to Ω_u. This distribution reflects the diminishing probability of finding a chain stretched close to its contour length due to a significant reduction in entropy. In the limit of $N \to \infty$, eq 31 converges to the Gaussian distribution predicted by a random walk in three dimensions. We therefore expect this distribution to be particularly relevant for networks of short chains ($N \sim 10$). Figure 5 illustrates a comparison of these distributions for $N = 15$ and $N = 30$, respectively. We see that the proposed distribution results in a higher likelihood of finding a coiled chain, as expected.

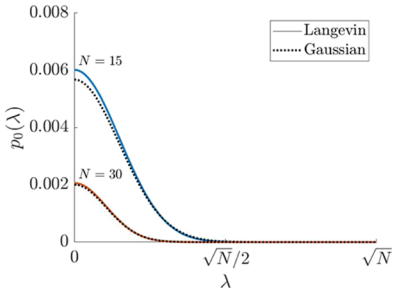

Figure 5. Comparison of the proposed distribution based on Langevin chain statistics (solid lines) with the distribution based on Gaussian chain statistics (black dotted lines) for networks with chains composed of $N = 15$ Kuhn segments and $N = 30$ Kuhn segments.

3.3. Network Damage and Self-Healing. Let us now concentrate on the model at the network level. When the network is undamaged and in a steady state, the kinetic rates of chain attachment and detachment, k_a and k_d, respectively, lead to an equilibrium concentration of chains C_0 that can be determined by enforcing $\dot{C}_d = 0$ in eq 10. This immediately yields

$$C_0 = C_{tot}\frac{k_a}{k_a + k_d} \tag{32}$$

By inserting eq 32 into eq 18, it can be immediately observed that the Clausius−Duhem inequality is satisfied at equilibrium. This concentration has a twofold effect on the network's response: (a) it determines its initial shear modulus via the relation $G_0 = C_0 kT$ and (b) it provides a limit to the number of chains that can be broken at any given time. For instance, if the detachment rate is greater than the attachment rate, then only a small fraction of the total chain population is connected to the network at equilibrium. In this scenario, only the effective chains are able to rupture and dissipate energy by chain scission. Therefore, we can define a meaningful network damage parameter d as the fraction of chains that have ruptured out of the entire total chain population. Specifically,

$$d = C_r/C_{tot} \tag{33}$$

From its definition, d varies from 0 (no chains have ruptured) to 1 (all chains have ruptured). We note here that this parameter does not provide a measure of effective network damage but rather a measure of the fraction of the chains (relative to the initial chain population) that can be used to carry load at later times. Furthermore, if the network has sustained damage, the steady-state concentration of effective chains (which was originally C_0) decreases to a value C_{eq} determined by

$$C_{eq} = (1 - d)C_0 \tag{34}$$

This new steady-state concentration determines the shear modulus of the network, $G = (1 - d)C_0 kT = (1 - d)G_0$. Since d is defined in terms of the total concentration of chains C_{tot}, rather than the initial concentration of effective chains C_0, the kinetic rates k_a and k_d effectively govern the amount of damage a dynamic network could attain when loaded quickly. For instance, if the network ruptures 50% of its initial chain population, the incremental change in damage will vary depending on the ratio C_0/C_{tot}. This stems from the fact that only elastically effective chains can rupture. The consequences of this predicted phenomenon are discussed further in Sections 3.5 and 4.

3.4. Numerical Solution. In the remainder of this work, we concentrate on predicting the mechanical response—elasticity, relaxation, and damage—of a polymer specimen that is subjected to a macroscopic deformation gradient $\boldsymbol{F}(t)$ whose time history is known but arbitrary. To facilitate visualization and numerical convenience, we will restrict our analysis to a two-dimensional chain conformation space for the duration of this paper, noting that the qualitative trends of the model are not affected. For this, the solution procedure can be summarized by three main steps:

1 Compute the evolution of the chain distribution ϕ by solving the Fokker−Planck equation introduced in eqs 5 and 6. This is accomplished numerically by solving the corresponding partial differential equation on a two-dimensional domain Ω_u, with $\boldsymbol{\lambda} = [\lambda_1, \lambda_2]$, $|\boldsymbol{\lambda}| < \lambda_c$. For this, we discretize the domain Ω_u as a circle of radius λ_c and solve eq 5 as a system of coupled ODEs. Note that the condition of $\mathbf{j}\cdot\mathbf{n} \geq 0 \in \Gamma$ is enforced numerically.

2 Compute the chain flux through the domain boundary, as shown in eq 9, in order to estimate the overall chain damage. As the instantaneous deformation of chains is affine according to the velocity gradient, chains which are stretched past the critical stretch λ_c in the previous step are considered to break before given the chance to

https://doi.org/10.1021/acs.macromol.1c01943
Macromolecules 2021, 54, 10801−10813

detach. The incremental change in ruptured chains $\delta C_r = \dot{C}_r \delta t$ is simply calculated by numerically integrating over the domain of chains with $|\lambda| \geq \lambda_c$.

3 Compute the stress tensor using the virial formula in eq 15. This is accomplished by assigning each chain a corresponding elastic force, given by eq 23, which depends on both the chain stretch λ and Kuhn segment stretch λ_b. We then use trapezoidal integration over the domain to compute the stress tensor.

To explore the prediction of this model, the remainder of this paper explores the role of various conditions (loading conditions and material parameters). In this context and to clarify our approach, we summarize the key parameters of the model in Table 1.

Table 1. Model Parameters

parameter	description	units
C	chain density	chains/volume
N	chain length	Kuhn segments
k_d	detachment rate	chains/second
k_a	attachment rate	chains/second
$(\mathcal{U}_b)_c$	critical bond energy	energy
E_b	bond stiffness	energy

3.5. Illustration. The proposed model provides a physically based procedure for differentiating between reversible chain detachment and irreversible chain rupture. In traditional covalently bonded networks, irreversible detachment dominates network softening as the cross-linking junctions are too strong to dissociate and reassociate at appreciable rates. However, networks that contain a large portion of physical bonds (e.g., hydrogen bonding, van der Waals forces, and so forth) present a coupling between these two processes that is governed by the loading rate and relative strength of the physical and chemical bonds present in the network. To remain general in our approach, we choose to describe these quantities with non-dimensional variables. We therefore introduce the Weissenberg number W, which expresses a normalized timescale relating the rate of deformation to the rate of elastic dissipation. In this study, we define it as

$$W = \frac{|\mathbf{L}|}{k_d} \tag{35}$$

where $|\boldsymbol{L}|$ is the spectral norm of the velocity gradient. For uniaxial tension experiments, this is the stretch rate $\dot{\lambda}$, while for simple shear, it is the shear rate $\dot{\gamma}$. When W is large, the network behaves elastically as most chains do not have time to detach during loading. In contrast, a low value of W would imply that chains stretch very little before detaching, which results in a more fluid-like response.

At this point, we seek to determine the observable effects of the intrinsic timescales in our system. With this objective, we consider a typical stress relaxation experiment in which a network is pulled in uniaxial tension at a loading rate $\dot{\lambda} \gg k_d$ (high W) to a pre-determined stretch λ_{max} and then held indefinitely to relax (Figure 6). During the loading phase, the attached and non-ruptured chains behave elastically but begin to rupture as they are pulled past the damage surface $|\lambda| = \lambda_c$. During the relaxation phase, two processes occur simultaneously to bring the network to its new equilibrium: (i) the detachment of stretched chains, resulting in energy dissipation and stress relaxation, and (ii) the attachment of chains from the detached population, sourcing self-healing and an increase in the nominal chain concentration C. The model is able to analytically capture the stress $\boldsymbol{\sigma}$ and nominal chain concentration C during network relaxation. We particularly note that the characteristic timescale of relaxation, $\tau_r = 1/k_d$, is independent of the kinetic rate of chain attachment as chains reattach in a stress-free state. Conversely, the timescale of self-healing, $\tau_h = 1/(k_a + k_d)$, involves both kinetic rates. These timescales are verified analytically in the Supporting Information. Thus, we expect the same normalized stress response as indicated in Figure 6a for networks with the same k_d, but the observed recovery in C will vary for different values of k_a (Figure 6b).

Let us now explore the effect of loading rate in the context of a cyclic loading simulation. In a damage-free elastic network, the loading and unloading curves are expected to follow the same path. When chains begin to rupture, however, the elastic

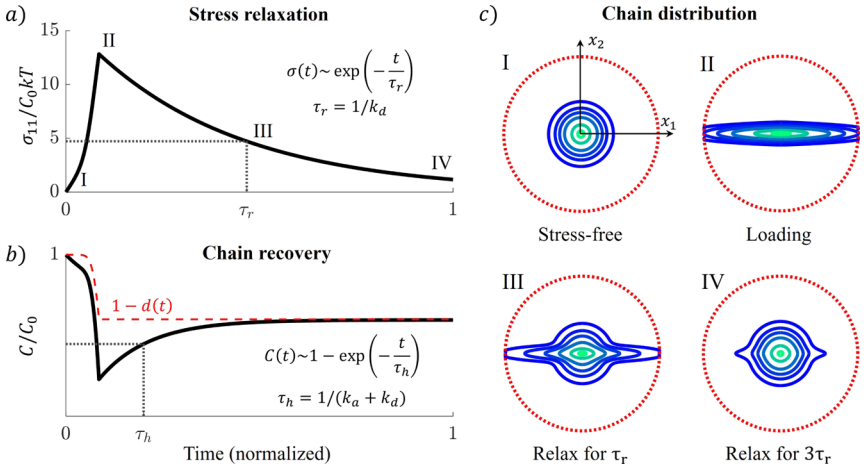

Figure 6. Stress relaxation experiment. (a) Normalized Cauchy stress vs normalized time. I–II is loaded at a constant rate of $\dot{\lambda} \gg$ kd. II–IV are held at a constant stretch. The time constant τ_r is indicated when stress has relaxed by ≈63%. (b) Chain concentration as a function of time. Note that the time constant of healing τ_h is not equal to that of relaxation. (c) Contour plots of the distribution ϕ at indicated time intervals. At longer times, the model predicts convergence to its initial state as $\phi(\mathbf{r}, t \to \infty) = (1 - d)\phi_0(\mathbf{r})$.

https://doi.org/10.1021/acs.macromol.1c01943
Macromolecules 2021, 54, 10801−10813

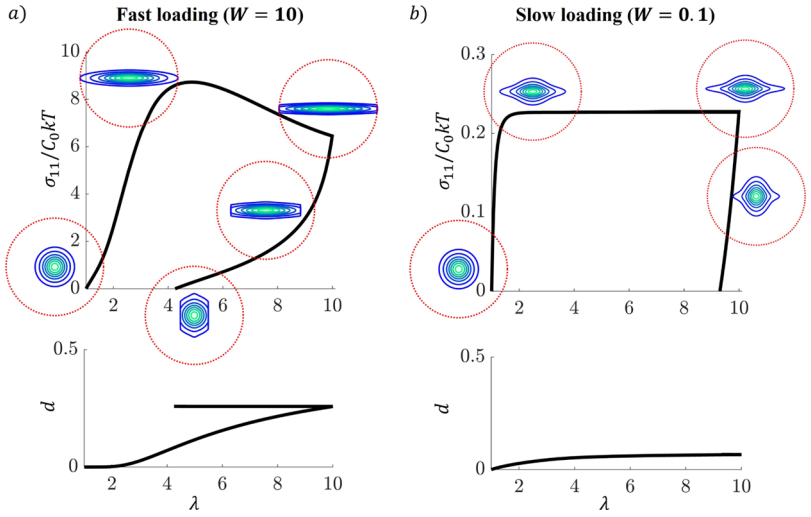

Figure 7. Cyclic loading experiment performed at a constant strain rate $\dot{\lambda}$. (a) High Weissenberg loading. Energy dissipation is primarily a result of chain rupture. (b) Low Weissenberg loading. Energy dissipation is primarily due to reversible bond kinetics. Contour plots indicate the distribution ϕ at the respective stage of loading.

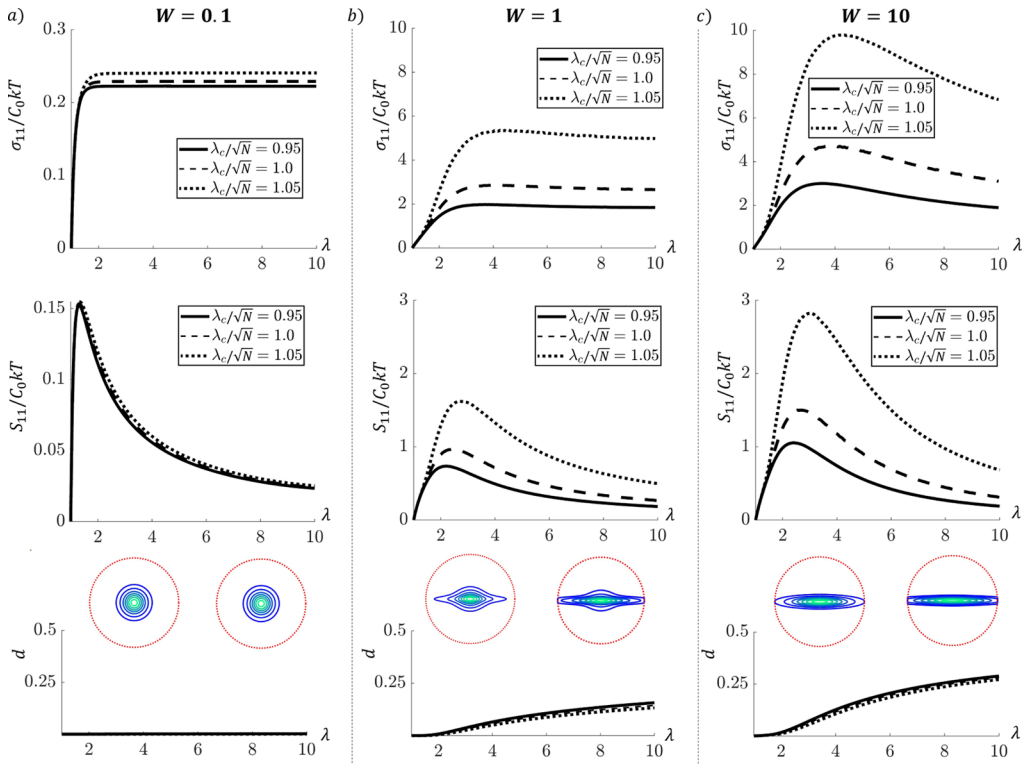

Figure 8. Uniaxial tension behavior for small loading rates (a), moderate loading rates (b), and high loading rates (c). First row is the true (Cauchy) stress, while the second row is the nominal stress (both in units of C_0kT). Note that the tick mark values in the y-axis of the first column are different from those in the second and third columns.

energy stored in the chain is lost, creating a distinct hysteresis loop. The presented model captures this effect in the limit of large W (Figure 7a). In this case, all the dissipated energy is due to chain rupture, and the resulting network damage is significant. Initially, the distribution $\phi(\boldsymbol{r})$ (illustrated as iso-contours over the two-dimensional chain conformation space in Figure 7) stretches affinely with loading. This creates a stiffening stress−strain response as a larger portion of chains approach their nonlinear regime near the contour length. At a certain point, a significant portion of chains cross the damage surface, illustrated by the red dashed circle of diameter λ_c, effectively softening the network. With further loading, the stress begins to decrease as more energy is released due to chain rupture than is stored elastically. The network is unloaded elastically as well, creating a distinct cutoff in the distribution in directions where chain rupture has occurred.

When viscous forces dominate (low W), energy dissipation is due to bond exchange and topological rearrangement (Figure 7b). Chains are typically not stretched far before detaching, and the stress response is much softer. Damage accumulation in this network reflects the creep-like response at high deformations; there is initially a small portion of chains

https://doi.org/10.1021/acs.macromol.1c01943
Macromolecules 2021, 54, 10801−10813

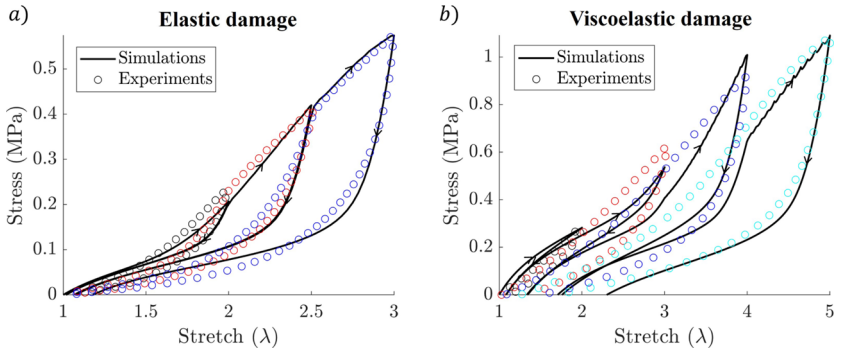

Figure 9. Multiple cyclic loading experiments. (a) PVA gels synthesized by Zhang et al.;[46] the response is primarily elastic, with energy dissipation due to chain rupture. (b) Metal-coordinated PAM hydrogels created by Ding et al.[48] Energy dissipation is due to chain rupture and bond exchange.

that rupture from their resting state being close to the damage surface, but this fraction of chains progressively becomes smaller as loading continues. Network evolution consists of incremental stretches, followed by detachment and reattachment events, which effectively reset the loading history. After a certain point, the initial conformation of chains is so far from the damage surface that no more damage is accumulated. This is accompanied by steady-state creep and a plateauing of the fraction of ruptured chains. We particularly note the unloading curve in Figure 7b, which reaches zero stress long before the material is unloaded completely, indicating a plastic deformation due to topological changes. The energy dissipation mechanisms in these networks are therefore quite different from those of an elastic network. We expect most real networks to exhibit both types of response, which yields more complicated behaviors due to the coupling of bond exchange, elastic deformation, and chain rupture. This is explored in the following section.

4. RESULTS AND DISCUSSION

The model presented in the previous sections serves as a foundation for describing polymer networks that undergo both reversible bond detachment and irreversible chain rupture. In many systems, weak physical bonds between neighboring chains source reversible detachment events in the form of hydrogen bonding or van der Waals forces, even if the network itself is held together by covalent junctions. In contrast, physically bonded polymers may experience chain scission when loaded at a rate much faster than the natural rate of bond exchange. These two mechanisms thus appear simultaneously in many materials that do not behave ideally. In this section, we summarize the basic predictions of the proposed model and provide relevant material examples where appropriate.

4.1. Basic Predictions. We begin a quantitative exploration of the model by considering a uniaxial tension experiment at a constant strain rate $\dot{\lambda}$. To illustrate the interplay between elasticity and viscoelasticity, we choose a range of Weissenberg numbers and critical stretches λ_c that fully explore the parametric space of the model. In particular, we choose three distinct values of λ_c corresponding to chains breaking when stretched slightly less than, equal to, or slightly greater than their inextensible contour length Nb. The strain rate is varied to represent networks that are primarily viscous ($W = 0.1$), primarily elastic ($W = 10$), or viscoelastic ($W = 1$). The results from nine simulations are summarized in Figure 8.

At low Weissenberg numbers, the material flows indefinitely in steady-state creep. An initial increase in stress is induced due to the sudden onset of deformation (Figure 8a). Very little change occurs to the distribution ϕ as rapid bond dynamics causes chains to detach before deforming. Almost no damage is accrued in the network as most chains detach before they are stretched to the point of rupture. Due to this, the critical stretch λ_c has very little effect on the predicted response. As we increase the Weissenberg number, however, the three curves begin to separate due to the highly nonlinear force response at large stretches (Figure 8b,c). In these networks, the elastic deformation competes with bond exchange, which induces a preferred alignment of chains in the direction of loading (illustrated by the iso-contour plots of the distribution ϕ). At larger stretches, a significant portion of chains approach the damage surface defined by λ_c (indicated by red circles in Figure 8) and rupture. In the case of $W = 1$ (Figure 8b), detachment events are ongoing at a comparable rate to the elastic distortion. Thus, a portion of chains are able to detach from their stretched state and reattach in the initial conformation before rupturing. Eventually, the incremental number of chains reversibly detaching becomes greater than the number of chains rupturing, and the damage and true stress plateau to equilibrium values. This is not the case for high Weissenberg loading, however, as chains deform elastically and do not have time to detach from the network before reaching their critical stretch (Figure 8c). In this case, the full population of initially effective chains, captured by C_0, is expected to fracture with increased loading. We note, however, that the concentration of detached chains, C_d, remains fully intact. Thus, the network is still expected to recover a portion of its elasticity when unloaded.

4.2. Viscoelasticity and Damage. The existence of time-dependent dissipative quantities (such as bond kinetics) is expected to have significant implications on the damage accumulation in a material undergoing repeated cyclic loading. On one hand, if the network can rearrange its topology completely during one cycle (a low Weissenberg number), there should be little to no chain rupture and thus no progressive softening of the network. The other extreme would pertain to permanent networks without dynamic bonds, which would continue to weaken with increased loading and increased strain. In this section, we demonstrate the presented model to unify these extremes as limiting cases relating to the Weissenberg number.

We here expand on the illustration in Figure 7 by simulating a step-cycle uniaxial loading experiment in which the network is immediately reloaded to a higher strain following the first unloading. Two mechanisms source energy dissipation in the

https://doi.org/10.1021/acs.macromol.1c01943
Macromolecules 2021, 54, 10801−10813

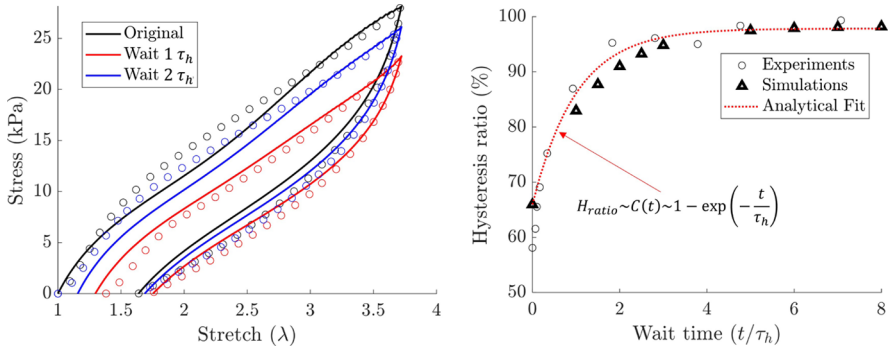

Figure 10. Self-healing experiments performed by Fang et al.[51] Left: cyclic loading curves performed with normalized wait times $\tau_h = 1$ and $\tau_h = 2$ after original loading. Right: Hysteresis ratio versus normalized wait time. The fitted curve is an exponential decay curve with a characteristic timescale $\tau_h = 1/(k_a + k_d)$, where τ_h was calculated from experimental calibration.

system: (i) the detachment of deformed chains and (ii) the rupture of highly stretched chains. For the limiting cases of low and high Weissenberg loading, the former and latter mechanisms dominate, respectively, and are each solely responsible for the dissipated energy in each respective case (appearing as a hysteresis loop as in Figure 7). It is difficult to decouple these contributions at moderate loading rates, however, as these two processes may be occurring simultaneously.

Let us start by considering a simulation performed at a high Weissenberg number. In this regime, we expect chain rupture to source all energy dissipation and the response of the intact network to be perfectly elastic. As bond rupture is irreversible, the unloading path is different from the loading path for a given cycle if damage has accrued during that cycle. However, chains cannot rupture during unloading, causing the following loading path to follow the previous unloading path perfectly. This reflects the fact that there are no inelastic changes to the distribution ϕ at high Weissenberg numbers; the same chains are continuously pulled in cycles until they reach their contour length and break. We would expect this type of response from networks with either very slow dynamics or chemical networks such as conventional elastomers and hydrogels. Indeed, a comparison to the data by Zhang et al.[46] reveals a nearly ideal elastic response with little to no fatigue and negligible viscoelastic dissipation throughout the loading history (Figure 9a). For this experiment, we fit the data with a Weissenberg number of $W = 100$, a chain length of $N = 10$, and a critical stretch of $\lambda_c/\sqrt{N} = 1.08$. The resolution of the TNT for chemical networks such as this can be interpreted by the timescales of attachment and detachment approaching zero ($k_d \rightarrow 0$), at which point the foundational model (without damage) has been shown to converge to the neo-Hookean model[31,47] and the statistically based elastic damage model described in Vernerey et al.[17]

The modification of this experiment for moderate loading rates ($W \approx 1$) yields different qualitative trends in the stress–strain relationship. At this loading rate, the timescale of dissipation by reversible bond exchange is significant, creating a visco-plastic response due to the added dissipative mechanism. We begin to see larger deviations of the loading and unloading curves—both within the same cycle and between subsequent cycles. The chains that were once stretched have either ruptured or exchanged their bonds to reattach in a stress-free conformation. Due to this, the concentration of stretched chains has decreased. This type of response is, in fact, more commonly observed in experimental systems. To explain this, we consider the fact that most hydrogels exhibit some form of rate-dependent behavior—whether it be from bond dynamics, solvent exudation, reptation of entanglements, and so forth. Even though the underlying physics governing each microscopic source to viscoelastic behavior is different, we expect the expression of the timescale for each phenomenon at the macroscale to be similar. With this caveat, a number of physical networks (whose primary source of viscoelasticity is due to bond dynamics) have been shown to exhibit similar behaviors to that predicted by the model.[49,50] For instance, the trends observed by Ding et al.[48] for an ionic polymer network match the qualitative predictions of the model (Figure 9b). We particularly note the distinct discontinuity observed between each loading cycle, which is commonly observed in viscoelastic polymers, but is not captured by many existing models. Thus, while the current formulation does not match all the trends in the data (in particular, the strong overlap between subsequent loading cycles), the combination of damage and viscoelasticity supplements our current state of modeling these experiments. This fitting predicts the kinetic rates to be $k_a = 6.9\ \text{ms}^{-1}$ and $k_d = 13.9\ \text{ms}^{-1}$, $N = 32$, and a critical stretch of $\lambda_c/\sqrt{N} = 1.1$.

4.3. Chain Reattachment and Self-Healing. Reversible bond detachment provides an intrinsic self-healing mechanism in physical networks, making them desirable for a variety of applications in biomedical and tissue engineering. The self-healing properties of a material are dictated by the kinetic rate of bond exchange as well as the concentration of reversible cross-linking junctions in the network. The kinetic rate of bond exchange is specific to the material and bond type, whereas the concentration of reversible cross-links may change with loading history. For instance, extreme loading conditions that have induced chain rupture may decrease the population of chains available for bond exchange. In this case, the network may only recover a portion of its stiffness and energy dissipation properties. To measure this in material systems, many researchers have performed subsequent cyclic loading experiments separated by a given wait time, t_w, and calculated the resulting hysteresis ratio for that test. The hysteresis ratio is defined as the energy dissipated during the loading–unloading cycle after the hold-and-wait time divided by the energy dissipated during the cycle prior to the hold-and-wait time (note that the energy dissipated by the material system during a cycle is equal to the area under the loading–unloading stress–strain curve). For small t_w, the network may retain

https://doi.org/10.1021/acs.macromol.1c01943
Macromolecules 2021, 54, 10801−10813

plastic strains and preferred chain alignment, and the stiffness and amount of energy dissipation may be smaller than the initial loading. As the wait time is increased, the network distribution ϕ approaches its original value, and the material properties approach those of the original network.

To further illustrate this point, we consider such a self-healing experiment performed by Fang et al. on a highly elastic protein hydrogel.[51] Their network is approximated by this model as a collection of unfolded proteins held together by physical cross-links. They discovered significant hysteresis loops and high toughness due to the energy dissipated from the folding and unfolding of proteins. Notably, the self-healing curve, measured by the hysteresis ratio versus wait time between cycles, closely follows the exponential trend of chain recovery illustrated in Figure 6. To confirm this, we fit the rate of chain detachment, k_d, to the initial loading curve by simulating this cycle at a constant applied velocity. From here, we determined k_a by fitting an exponential curve to the self-healing curve with a characteristic time $\tau_h = 1/(k_a + k_d)$. As illustrated in Figure 10, the model shows excellent agreement with the self-healing behavior of the material using model parameters $k_a = 51.9\ \mathrm{ms}^{-1}$, $k_d = 148\ \mathrm{ms}^{-1}$, $N = 26$, and $\lambda_c/\sqrt{N} = 1.0$. We thus expect that the recovery of the hysteresis ratio closely aligns with a recovery of the chain concentration toward its new equilibrium value. Similar experiments were performed by many researchers,[48,52−54] each of whom reported an exponential recovery in hysteresis ratio with respect to wait time. We finally note that the model predicts recovery to be proportional to the damage accrued in the network during its initial loading; thus, the equilibrium value of the hysteresis ratio indicates the fraction of chains that have irreversibly ruptured in the network. For this experiment, we predict that roughly 5% of the initial chain concentration has ruptured as the hysteresis ratio approaches 95%.

5. SUMMARY

In dynamic polymer networks, the mechanisms of reversible bond exchange and irreversible chain rupture occur simultaneously, resulting in a complex response with multiple governing timescales. This poses significant challenges in modeling the behavior of these networks as the characteristics of their response may be due to one or both of these network degrading processes. In this paper, we have presented a micromechanically based formulation for describing dynamic polymer networks whose chains rupture when stretched past a critical stretch. A statistical description of the network is used based on the TNT, which allows the model to bridge macroscopic quantities such as stress and stored energy to the conformation space of a representative chain. To capture bond rupture, we incorporate an enthalpic term into the free-energy density, which accounts for bond stretching and eventual rupture at high chain stretches. The model predicts several responses characteristic of physical networks, including rate-dependence, strain stiffening, and self-healing.

Two timescales are found to govern the behavior of a simple dynamic polymer network: the timescales of relaxation and self-healing. Even though these timescales are related to the kinetic rates of bond association and dissociation, they are not necessarily of comparable magnitudes. The relaxation timescale, which is responsible for rate dependence and energy dissipation, is strictly governed by the kinetic rate of dissociation. The timescale of self-healing, however, is inversely proportional to the summed rate of chain attachment and detachment. This finding has considerable implications especially when considering bond rupture and network damage since only "elastically effective" chains (i.e., not dangling chains) can be ruptured during a loading cycle. Furthermore, based on the results in Section 4.3, we may propose a simple method for approximating these rates experimentally with two common setups. First, a relaxation test may be performed to determine the characteristic relaxation time $\tau_r = 1/k_d$, as is already common for viscoelastic materials. Second, a self-healing experiment may be performed by measuring the recovery of the hysteresis ratio under cyclic loading. The timescale of self-healing $\tau_h = 1/(k_a + k_d)$ can then be calculated approximately by an exponential fitting. By measuring these rates, it could be possible to tune the desired properties, such as initial shear modulus, self-healing behavior, and chain extensibility, for a desired application.

The presented formulation rests upon several assumptions that may be revised according to the type of network studied. One of the primary assumptions, as mentioned in Section 2, is the instantaneously affine kinematic law. In many experimental systems, this has been shown to break down at high strains, where it is hypothesized that alternative mechanisms such as reptation are energetically preferred. For this model, this could be reflected by applying a non-affine kinematic law for highly stretched conformations of ϕ. Furthermore, the numerical implementation presented in this work is highly simplified due to the use of a two-dimensional chain conformation space. This is due to the limitations of tracking the full three-dimensional chain conformation space at each stage of loading, which is computationally expensive. We emphasize the intention of this work to provide a qualitative understanding of the governing physics outlined in Section 2 and note that a more sophisticated numerical strategy could mitigate this. For instance, reducing the model to the domain of a microsphere[37,55,56] could significantly reduce computational cost and open the possibility for implementation in finite element method models. We finally note that our usage of a first-order kinetic law, with constant rates of k_a and k_d, does not account for the force sensitivity of bond lifetime in many physical systems.[36] The model may therefore be supplemented by including a functional form of k_d on the force f in the chain as per previous works.[37] Relaxing some of these assumptions is expected to yield better fittings for the experimental comparisons presented in this work. In particular, the Mullins-like effect observed in Figure 9b that was not captured by this model has been explained by other researchers by network alteration[56] (reflecting the changes of non-affine deformation) as well as nonlinear viscoelasticity.[37]

Dynamic polymers have been praised for their ability to toughen gels and increase their extensibility.[57,58] This is commonly attributed to the reversible cross-links acting as "sacrificial" bonds, which dissipate energy that would otherwise be stored in an elastic network. The framework presented here could have significant implications on the localization and propagation of fracture in these materials as tracking the full chain distribution defines an innate length scale that is otherwise lost in empirical continuum models. In particular, this model accounts for the preferred rupture of highly stretched chains at a single point in space, which could help to explain the zone surrounding the crack tip of a viscoelastic material—a topic that is still poorly understood.[10,59,60] Furthermore, the diffusive motion of dynamic chains into a

https://doi.org/10.1021/acs.macromol.1c01943
Macromolecules 2021, 54, 10801−10813

localized region of damage could be incorporated into this framework to explain more complex patterns of self-healing, such as mending a material which has been cut in half entirely.[61] This would also be relevant for the interplay between reptation and damage in elastomers, as well as hydrogels with slideable cross-links.[62,63]

■ ASSOCIATED CONTENT

Supporting Information

The Supporting Information is available free of charge at https://pubs.acs.org/doi/10.1021/acs.macromol.1c01943.

Analytical derivations for the timescales of relaxation $\tau_r = 1/k_d$ and self-healing $\tau_h = 1/(k_a + k_d)$ (PDF)

■ AUTHOR INFORMATION

Corresponding Author

Franck J. Vernerey − *Department of Mechanical Engineering, University of Colorado Boulder, Boulder, Colorado 80309, United States;* orcid.org/0000-0001-6138-1431; Email: franck.vernerey@colorado.edu

Authors

Samuel C. Lamont − *Department of Mechanical Engineering, University of Colorado Boulder, Boulder, Colorado 80309, United States*

Jason Mulderrig − *Sibley School of Mechanical and Aerospace Engineering, Cornell University, Ithaca, New York 14853, United States*

Nikolaos Bouklas − *Sibley School of Mechanical and Aerospace Engineering, Cornell University, Ithaca, New York 14853, United States*

Complete contact information is available at: https://pubs.acs.org/10.1021/acs.macromol.1c01943

Notes

The authors declare no competing financial interest.

■ ACKNOWLEDGMENTS

F.J.V. gratefully acknowledges the support of the National Science Foundation under award no. 1761 918. J.M. gratefully acknowledges the support of the National Science Foundation Graduate Research Fellowship Program under grant no. DGE-1650 441. Any opinions, findings, and conclusions or recommendations expressed in this material are those of the author(s) and do not necessarily reflect the views of the National Science Foundation. F.J.V. and S.C.L. acknowledge support by the Department of Energy, National Nuclear Security Administration, Predictive Science Academic Alliance Program (PSAAP), under award number DE-NA0003962. This report was prepared as an account of work sponsored by an agency of the United States Government. Neither the United States Government nor any agency thereof, nor any of their employees, makes any warranty, express or implied, or assumes any legal liability or responsibility for the accuracy, completeness, or usefulness of any information, apparatus, product, or process disclosed, or represents that its use would not infringe privately owned rights. Reference herein to any specific commercial product, process, or service by trade name, trademark, manufacturer, or otherwise does not necessarily constitute or imply its endorsement, recommendation, or favoring by the United States Government or any agency thereof. The views and opinions of authors expressed herein do not necessarily state or reflect those of the United States Government or any agency thereof.

■ REFERENCES

(1) Coyle, S.; Majidi, C.; LeDuc, P.; Hsia, K. J. Bio-inspired soft robotics: Material selection, actuation, and design. *Extreme Mech. Lett.* **2018**, *22*, 51−59.

(2) Akalp, U.; Bryant, S. J.; Vernerey, F. J. Tuning tissue growth with scaffold degradation in enzyme-sensitive hydrogels: a mathematical model. *Soft Matter* **2016**, *12*, 7505−7520.

(3) Bryant, S. J.; Vernerey, F. J. Programmable Hydrogels for Cell Encapsulation and Neo-Tissue Growth to Enable Personalized Tissue Engineering. *Adv. Healthc. Mater.* **2018**, *7*, 1700605.

(4) Haque, M. A.; Kurokawa, T.; Gong, J. P. Super tough double network hydrogels and their application as biomaterials. *Polymer* **2012**, *53*, 1805−1822.

(5) Lin, S.; Yuk, H.; Zhang, T.; Parada, G. A.; Koo, H.; Yu, C.; Zhao, X. Stretchable Hydrogel Electronics and Devices. *Adv. Mater.* **2016**, *28*, 4497−4505.

(6) Agrawal, S.; Singh, K. K.; Sarkar, P. Impact damage on fibre-reinforced polymer matrix composite—A review. *J. Compos. Mater.* **2014**, *48*, 317−332.

(7) Moutos, F. T.; Freed, L. E.; Guilak, F. A biomimetic three-dimensional woven composite scaffold for functional tissue engineering of cartilage. *Nat. Mater.* **2007**, *6*, 162−167.

(8) Gong, J. P.; Katsuyama, Y.; Kurokawa, T.; Osada, Y. Double-Network Hydrogels with Extremely High Mechanical Strength. *Adv. Mater.* **2003**, *15*, 1155−1158.

(9) Millereau, P.; Ducrot, E.; Clough, J. M.; Wiseman, M. E.; Brown, H. R.; Sijbesma, R. P.; Creton, C. Mechanics of elastomeric molecular composites. *Proc. Natl. Acad. Sci.* **2018**, *115*, 9110−9115.

(10) Mayumi, K.; Guo, J.; Narita, T.; Hui, C. Y.; Creton, C. Fracture of dual crosslink gels with permanent and transient crosslinks. *Extreme Mech. Lett.* **2016**, *6*, 52−59.

(11) Sun, J.-Y.; Zhao, X.; Illeperuma, W. R. K.; Chaudhuri, O.; Oh, K. H.; Mooney, D. J.; Vlassak, J. J.; Suo, Z. Highly stretchable and tough hydrogels. *Nature* **2012**, *489*, 133−136.

(12) Wu, J.; Cai, L.-H.; Weitz, D. A. Tough Self-Healing Elastomers by Molecular Enforced Integration of Covalent and Reversible Networks. *Adv. Mater.* **2017**, *29*, 1702616.

(13) Zhao, X.; Chen, X.; Yuk, H.; Lin, S.; Liu, X.; Parada, G. Soft Materials by Design: Unconventional Polymer Networks Give Extreme Properties. *Chem. Rev.* **2021**, *121*, 4309−4372.

(14) Hu, Y.; Du, Z.; Deng, X.; Wang, T.; Yang, Z.; Zhou, W.; Wang, C. Dual Physically Cross-Linked Hydrogels with High Stretchability, Toughness, and Good Self-Recoverability. *Macromolecules* **2016**, *49*, 5660−5668.

(15) Mao, Y.; Talamini, B.; Anand, L. Rupture of polymers by chain scission. *Extreme Mech. Lett.* **2017**, *13*, 17−24.

(16) Li, B.; Bouklas, N. A variational phase-field model for brittle fracture in polydisperse elastomer networks. *Int. J. Solids Struct.* **2020**, *182−183*, 193−204.

(17) Vernerey, F. J.; Brighenti, R.; Long, R.; Shen, T. Statistical Damage Mechanics of Polymer Networks. *Macromolecules* **2018**, *51*, 6609−6622.

(18) Guo, Q.; Zaïri, F. A micromechanics-based model for deformation-induced damage and failure in elastomeric media. *Int. J. Plast.* **2021**, *140*, 102976.

(19) Lavoie, S. R.; Long, R.; Tang, T. A rate-dependent damage model for elastomers at large strain. *Extreme Mech. Lett.* **2016**, *8*, 114−124.

(20) Lavoie, S. R.; Long, R.; Tang, T. Modeling the mechanics of polymer chains with deformable and active bonds. *J. Phys. Chem. B* **2019**, *124*, 253−265.

(21) Lake, G. J.; Thomas, A. G.; Tabor, D. The strength of highly elastic materials. *Proc. R. Soc. London, Ser. A* **1967**, *300*, 108−119.

(22) Talamini, B.; Mao, Y.; Anand, L. Progressive damage and rupture in polymers. *J. Mech. Phys. Solids* **2018**, *111*, 434−457.

(23) Mulderrig, J.; Li, B.; Bouklas, N. Affine and non-affine microsphere models for chain scission in polydisperse elastomer networks. *Mech. Mater.* **2021**, *160*, 103857.
(24) Lu, T.; Wang, Z.; Tang, J.; Zhang, W.; Wang, T. A pseudo-elasticity theory to model the strain-softening behavior of tough hydrogels. *J. Mech. Phys. Solids* **2020**, *137*, 103832.
(25) Xiao, R.; Han, N.; Zhong, D.; Qu, S. Modeling the mechanical behaviors of multiple network elastomers. *Mech. Mater.* **2021**, *161*, 103992.
(26) Green, M. S.; Tobolsky, A. V. A New Approach to the Theory of Relaxing Polymeric Media. *J. Chem. Phys.* **1946**, *14*, 80−92.
(27) Lodge, A. S. A network theory of flow birefringence and stress in concentrated polymer solutions. *Trans. Faraday Soc.* **1956**, *52*, 120−130.
(28) Linder, C.; Tkachuk, M.; Miehe, C. A micromechanically motivated diffusion-based transient network model and its incorporation into finite rubber viscoelasticity. *J. Mech. Phys. Solids* **2011**, *59*, 2134−2156.
(29) Bergström, J.; Boyce, M. C. Constitutive modeling of the large strain time-dependent behavior of elastomers. *J. Mech. Phys. Solids* **1998**, *46*, 931−954.
(30) Tanaka, F.; Edwards, S. F. Viscoelastic properties of physically crosslinked networks. 1. Transient network theory. *Macromolecules* **1992**, *25*, 1516−1523.
(31) Vernerey, F. J.; Long, R.; Brighenti, R. A statistically-based continuum theory for polymers with transient networks. *J. Mech. Phys. Solids* **2017**, *107*, 1−20.
(32) Buche, M. R.; Silberstein, M. N. Chain breaking in the statistical mechanical constitutive theory of polymer networks. *J. Mech. Phys. Solids* **2021**, *156*, 104593.
(33) Benaarbia, A.; Chatzigeorgiou, G.; Kiefer, B.; Meraghni, F. A fully coupled thermo-viscoelastic-viscoplastic-damage framework to study the cyclic variability of the Taylor-Quinney coefficient for semi-crystalline polymers. *Int. J. Mech. Sci.* **2019**, *163*, 105128.
(34) He, G.; Liu, Y.; Hammi, Y.; Bammann, D. J.; Horstemeyer, M. F. A combined viscoelasticity-viscoplasticity-anisotropic damage model with evolving internal state variables applied to fiber reinforced polymer composites. *Mech. Adv. Mater. Struct.* **2021**, *28*, 1775−1796.
(35) Vernerey, F. J. Transient response of nonlinear polymer networks: A kinetic theory. *J. Mech. Phys. Solids* **2018**, *115*, 230−247.
(36) Meng, F.; Pritchard, R. H.; Terentjev, E. M. Stress Relaxation, Dynamics, and Plasticity of Transient Polymer Networks. *Macromolecules* **2016**, *49*, 2843−2852.
(37) Lamont, S.; Vernerey, F. J. A Transient Microsphere Model for nonlinear viscoelasticity in dynamic polymer networks. *J. Appl. Mech.* **2021**, *89*, 011009.
(38) Wineman, A. On the mechanics of elastomers undergoing scission and cross-linking. *Int. J. Adv. Eng. Sci. Appl. Math.* **2009**, *1*, 123−131.
(39) Cohen, A. A Padé approximant to the inverse Langevin function. *Rheol. Acta* **1991**, *30*, 270−273.
(40) Kuhn, W.; Grün, F. Beziehungen zwischen elastischen Konstanten und Dehnungsdoppelbrechung hochelastischer Stoffe. *Kolloid-Z.* **1942**, *101*, 248−271.
(41) James, H. M.; Guth, E. Theory of the Elastic Properties of Rubber. *J. Chem. Phys.* **1943**, *11*, 455−481.
(42) *CRC Standard Mathematical Tables and Formulas*, 33rd ed.; Zwillinger, D.; Chapman and Hall/CRC: Boca Raton, 2018.
(43) Flory, P. J.; Rehner, J. Statistical Mechanics of Cross-Linked Polymer Networks I. Rubberlike Elasticity. *J. Chem. Phys.* **1943**, *11*, 512−520.
(44) Kuhn, W.; Grün, F. Statistical behavior of the single chain molecule and its relation to the statistical behavior of assemblies consisting of many chain molecules. *J. Polym. Sci.* **1946**, *1*, 183−199.
(45) Buche, M. R.; Silberstein, M. N. Statistical mechanical constitutive theory of polymer networks: The inextricable links between distribution, behavior, and ensemble. *Phys. Rev. E* **2020**, *102*, 012501.
(46) Zhang, L.; Zhao, J.; Zhu, J.; He, C.; Wang, H. Anisotropic tough poly(vinyl alcohol) hydrogels. *Soft Matter* **2012**, *8*, 10439−10447.
(47) Lalitha Sridhar, S.; Vernerey, F. The Chain Distribution Tensor: Linking Nonlinear Rheology and Chain Anisotropy in Transient Polymers. *Polymers* **2018**, *10*, 848.
(48) Ding, H.; Liang, X.; Zhang, X. N.; Wu, Z. L.; Li, Z.; Sun, G. Tough supramolecular hydrogels with excellent self-recovery behavior mediated by metal-coordination interaction. *Polymer* **2019**, *171*, 201−210.
(49) Jing, Z.; Dai, X.; Xian, X.; Du, X.; Liao, M.; Hong, P.; Li, Y. Tough, stretchable and compressive alginate-based hydrogels achieved by non-covalent interactions. *RSC Adv.* **2020**, *10*, 23592−23606.
(50) Zhang, Y.; Xue, J.; Li, D.; Li, H.; Huang, Z.; Huang, Y.; Gong, C.; Long, S.; Li, X. Tough hydrogels with tunable soft and wet interfacial adhesion. *Polym. Test.* **2021**, *93*, 106976.
(51) Fang, J.; Mehlich, A.; Koga, N.; Huang, J.; Koga, R.; Gao, X.; Hu, C.; Jin, C.; Rief, M.; Kast, J.; Baker, D.; Li, H. Forced protein unfolding leads to highly elastic and tough protein hydrogels. *Nat. Commun.* **2013**, *4*, 2974.
(52) Ding, H.; Zhang, X. N.; Zheng, S. Y.; Song, Y.; Wu, Z. L.; Zheng, Q. Hydrogen bond reinforced poly(1-vinylimidazole-co-acrylic acid) hydrogels with high toughness, fast self-recovery, and dual pH-responsiveness. *Polymer* **2017**, *131*, 95−103.
(53) Yu, H. C.; Zhang, H.; Ren, K.; Ying, Z.; Zhu, F.; Qian, J.; Ji, J.; Wu, Z. L.; Zheng, Q. Ultrathin k-Carrageenan/Chitosan Hydrogel Films with High Toughness and Antiadhesion Property. *ACS Appl. Mater. Interfaces* **2018**, *10*, 9002−9009.
(54) Ye, Y. N.; Cui, K.; Hong, W.; Li, X.; Yu, C.; Hourdet, D.; Nakajima, T.; Kurokawa, T.; Gong, J. P. Molecular mechanism of abnormally large nonsoftening deformation in a tough hydrogel. *Proc. Natl. Acad. Sci.* **2021**, *118*, No. e2014694118.
(55) Miehe, C.; Göktepe, S.; Lulei, F. A micro-macro approach to rubber-like materials—Part I: the non-affine micro-sphere model of rubber elasticity. *J. Mech. Phys. Solids* **2004**, *52*, 2617−2660.
(56) Diani, J.; Le Tallec, P. A fully equilibrated microsphere model with damage for rubberlike materials. *J. Mech. Phys. Solids* **2019**, *124*, 702−713.
(57) Ducrot, E.; Chen, Y.; Bulters, M.; Sijbesma, R. P.; Creton, C. Toughening Elastomers with Sacrificial Bonds and Watching Them Break. *Science* **2014**, *344*, 186−189.
(58) Miwa, Y.; Kurachi, J.; Kohbara, Y.; Kutsumizu, S. Dynamic ionic crosslinks enable high strength and ultrastretchability in a single elastomer. *Commun. Chem.* **2018**, *1*, 5.
(59) Creton, C.; Ciccotti, M. Fracture and adhesion of soft materials: a review. *Rep. Prog. Phys.* **2016**, *79*, 046601.
(60) Shen, T.; Vernerey, F. J. Rate-dependent fracture in transient networks. *J. Mech. Phys. Solids* **2020**, *143*, 104028.
(61) Yu, K.; Xin, A.; Wang, Q. Mechanics of self-healing polymer networks crosslinked by dynamic bonds. *J. Mech. Phys. Solids* **2018**, *121*, 409−431.
(62) Noda, Y.; Hayashi, Y.; Ito, K. From topological gels to slide-ring materials. *J. Appl. Polym. Sci.* **2014**, *131*, DOI: 10.1002/app.40509
(63) Vernerey, F. J.; Lamont, S. Transient mechanics of slide-ring networks: A continuum model. *J. Mech. Phys. Solids* **2021**, *146*, 104212.

https://doi.org/10.1021/acs.macromol.1c01943
Macromolecules 2021, 54, 10801−10813